Langmuir

Article

pubs.acs.org/Langmuir

High Performance Hydrogen Storage from Be-BTB Metal–Organic Framework at Room Temperature

Wei-Xian Lim,[†,‡] Aaron W. Thornton,*[,‡] Anita J. Hill,[‡] Barry J. Cox,[†] James M. Hill,[†] and Matthew R. Hill[‡]

[†]Nanomechanics Group, School of Mathematical Sciences, The University of Adelaide, SA 5005, Australia

[‡]CSIRO Material Science and Engineering and Process Science and Engineering, Private Bag 33, Clayton VIC 3169, Australia

Supporting Information

ABSTRACT: The metal–organic framework beryllium benzene tribenzoate (Be-BTB) has recently been reported to have one of the highest gravimetric hydrogen uptakes at room temperature. Storage at room temperature is one of the key requirements for the practical viability of hydrogen-powered vehicles. Be-BTB has an exceptional 298 K storage capacity of 2.3 wt % hydrogen. This result is surprising given that the low adsorption enthalpy of 5.5 kJ mol^{-1}. In this work, a combination of atomistic simulation and continuum modeling reveals that the beryllium rings contribute strongly to the hydrogen interaction with the framework. These simulations are extended with a thermodynamic energy optimization (TEO) model to compare the performance of Be-BTB to a compressed H_2 tank and benchmark materials MOF-5 and MOF-177 in a MOF-based fuel cell. Our investigation shows that none of the MOF-filled tanks satisfy the United States Department of Energy (DOE) storage targets within the required operating temperatures and pressures. However, the Be-BTB tank delivers the most energy per volume and mass compared to the other material-based storage tanks. The pore size and the framework mass are shown to be contributing factors responsible for the superior room temperature hydrogen adsorption of Be-BTB.

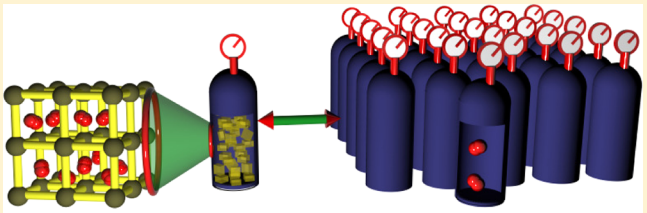

Hydrogen adsorption in MOF-based fuel tanks

1. INTRODUCTION

Storage of hydrogen gas is the key technological challenge in the development of hydrogen fuel cell vehicles. Hydrogen fuel cells are considered to be an environmental imperative, because they generate electricity with emissions of water and heat as compared to the carbon dioxide emissions generated when fossil fuels are used to produce electricity. In order for the technology to become competitive with existing vehicle fuels, in terms of cost and driving range, 5 kg of hydrogen is required to be stored on-board. Present compressed gas tank technology requires an exceptional compression to avoid prohibitive space requirements.[1] Storage capacities that approach the required amounts of hydrogen may only be achieved with conventional technology either through the use of high pressures or cryogenic temperatures.[2] There are limitations with the use of high pressures or cryogenic temperatures due to the increased system components that are required. Furthermore, the energy penalties associated with the compression and/or cooling of the hydrogen dramatically diminish the environmental benefits of employing hydrogen powered vehicles. The latest DOE Annual Merit Review of the Hydrogen Storage Sub-Program[3] concluded that physical sorbents are the leading candidates, with storage capacity and loss of usable hydrogen as the remaining challenges. Therefore, this work focuses on enhancing the storage capacity by using beryllium benzene tribenzoate (Be-BTB) with optimized operating conditions.

A gas in its adsorbed state can be stored at far greater densities in comparison with the bulk gas state. The use of novel nanostructured materials as adsorbents within a storage tank therefore offers the potential to increase the storage density through chemisorption or physisorption processes. Chemisorption relies on the formation of hydride chemical bonds within a material, whereas physisorption relies on van der Waals type interactions with internal surfaces of a porous material. The interaction strength of physisorbed gas molecules is primarily governed by local dipole moments induced in the hydrogen molecule by vacant point charges.[4]

The temperature at which hydrogen is adsorbed and desorbed is a key parameter of overall material performance. Temperature is embedded in the enthalpy of adsorption, which is the energy associated with the adsorption process. Theoretical calculations reveal that the ideal enthalpy of adsorption at room temperature, Q, is in the range of 15–25 kJ mol^{-1}.[5] Higher values are typically found in chemisorbents, which require heating to release stored hydrogen with only a fraction of the hydrogen released due to the strength of the chemical bond. The ability to cycle these chemisorbent materials is limited due to the significant change in the volume of the unit cell during the filling and emptying processes.

Received: December 13, 2012
Revised: June 6, 2013
Published: June 7, 2013

The inherent limitations of chemisorbents have led to an intense interest in physisorbents. These materials undergo no structural change on adsorption cycling and possess lower adsorption enthalpies. However, adsorption enthalpies are typically in the range of 5−10 kJ mol^{-1}, meaning that cryogenic temperatures are often required to reach high storage capacities. Keys to the optimization of performance of physisorbents are maximizing surface area, which is known to increase the storage capacity,[6] and the control of pore architecture and surface chemistry in order to maximize adsorption enthalpy.[7]

Metal−organic frameworks (MOFs) comprise metal atoms or clusters linked periodically by organic molecules to establish an array where each atom forms part of an internal surface. MOFs have delivered the highest surface areas and hydrogen storage capacities for any physisorbent and are shown to be a promising material for gas storage.[8] Exposed metal sites,[9,10] pore sizes,[11] and ligand chemistries[12,13] have been found to be the most effective routes for increasing the hydrogen enthalpy of adsorption within MOFs.

The MOF adsorbent that presently holds the record for gravimetric hydrogen storage capacity at room temperature is the first structurally characterized beryllium-based framework, Be-BTB (BTB = benzene tribenzoate); see Figure 1. Be-BTB has a Brunauer−Emmett−Teller (BET)[14] surface area of 4400 $m^2\ g^{-1}$, and Be-BTB can adsorb 2.3 wt % hydrogen at 298 K and 100 bar.[15] In the following subsection, the performance of Be-BTB is compared to other high performing MOFs.

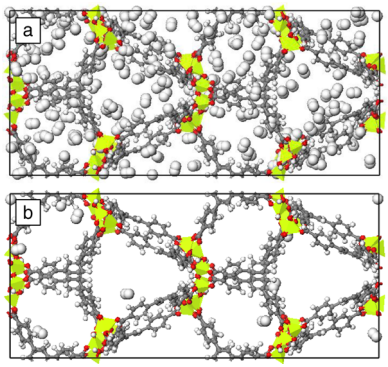

Figure 1. Molecular simulation snapshots of hydrogen (H_2) adsorption within the Be-BTB framework. (a) H_2 adsorbed at optimized storage conditions, 233 K and 100 bar. (b) H_2 remaining at DOE delivery conditions, 358 K and 5 bar.

1.1. Comparison with Other MOFs. With a focus on room temperature adsorption, we have collected data from the literature which has recently been summarized by Suh et al.[4] to compare the characteristics of Be-BTB with other MOFs. Only MOFs with reported pore volume and excess gravimetric uptake at 298 K and high pressures (more than 35 bar) are used for comparison with the Be-BTB. The total uptake is calculated using the method discussed by Frost and Snurr[16] (refer to the Supporting Information for more information). These MOFs are categorized as MOFs with open metal sites and MOFs without open metal sites. Data for MOFs with open metal sites are listed in Table S1 and data for MOFs without open metal sites are listed in Table S2 in the Supporting Information. MOFs with high density of open metal sites are shown to have better adsorption capability compared to MOFs without open metal sites at low pressures.[17] Figure 2 shows that this is also true at higher pressures with the exception of Be-BTB, which has the highest H_2 uptake of all the MOFs without open metal sites.

Frost and Snurr[16] studied the relationship between heat of adsorption, pore volume, and surface area with the total uptake at room temperature and various pressures. They found that these relationships depend on the strength of the interaction between H_2 and the porous material. For weak adsorption, the uptake correlates with the pore volume at all pressures. For a stronger adsorption, the uptake depends on the pressure where at low pressures the uptake correlates with the heat of adsorption, surface area at intermediate pressure, and pore volume at high pressures. This is verified through an analysis of the data in Figure 2 using the R software.[18] The lines of best fit for MOFs with and without open metal sites are shown in Figure 2 and the coefficient of determination of the total H_2 uptake with heat of adsorption, BET surface area, and pore volume are reported in Table 1.

For MOFs with open metal sites at 298 K and high pressures, the coefficient of determinant or R^2 calculated for the heat of adsorption, BET surface area, and pore volume are 0.23%, 91%, and 83%, respectively. This means that, with stronger adsorption, up to 91% and 83% of the variability of total uptake can be described by the BET surface area and pore volume, respectively. Similar to the findings of Frost and Snurr,[16] the heat of adsorption does not play a strong role in high pressures at room temperature for MOFs with open metal sites.

For MOFs without open metal sites, the R^2 values for the heat of adsorption, BET surface area, and pore volume are 1.43%, 7.22%, and 52.63%, respectively, which matches the results from Frost and Snurr[16] indicating that, for weak adsorption, the pore volume describes up to 52.63% of the variability of total uptake. We therefore conclude that the Be-BTB's superior uptake at room temperature is partly due to its high pore volume. Further, we will investigate the nature of this pore volume.

Gravimetric hydrogen adsorption in MOFs can be increased by substituting metals with lighter metals as shown by Porter et al.[19] where the zinc in zinc benzene dicarboxylate (MOF-5 or IRMOF-1) is substituted with beryllium to create beryllium benzene dicarboxylate (Be-BDC). In the case of Be-BTB, the lower density provided through the use of lightweight beryllium atoms does not account for the exceptional hydrogen adsorption performance,[15] as MOFs with higher gravimetric surface areas exhibit far lower room temperature storage capacities.[16]

Hydrogen adsorbents are often compared with reference to their volumetric or gravimetric capacity alone. However, to completely assess their potential to outperform current technologies, an analysis of their cyclability must also be considered. The assessment must incorporate the energy required to regenerate the material whether that be by temperature swing, pressure swing, or a combination of both. As each MOF exhibits its own unique isotherm behavior, the optimal cycle conditions (i.e., adsorption/desorption or store/release conditions) are also unique. Hence, here we adopt a thermodynamic energy optimization (TEO) model to determine the optimal cycle conditions of an empty compressed gas tank and a tank filled with Be-BTB, MOF-5 (IRMOF-1), or MOF-177.

The objectives of this work are to explain the high performance of Be-BTB as a room temperature adsorbent, to place in context the prevailing views on the contributions of

dx.doi.org/10.1021/la401446s | Langmuir 2013, 29, 8524−8533

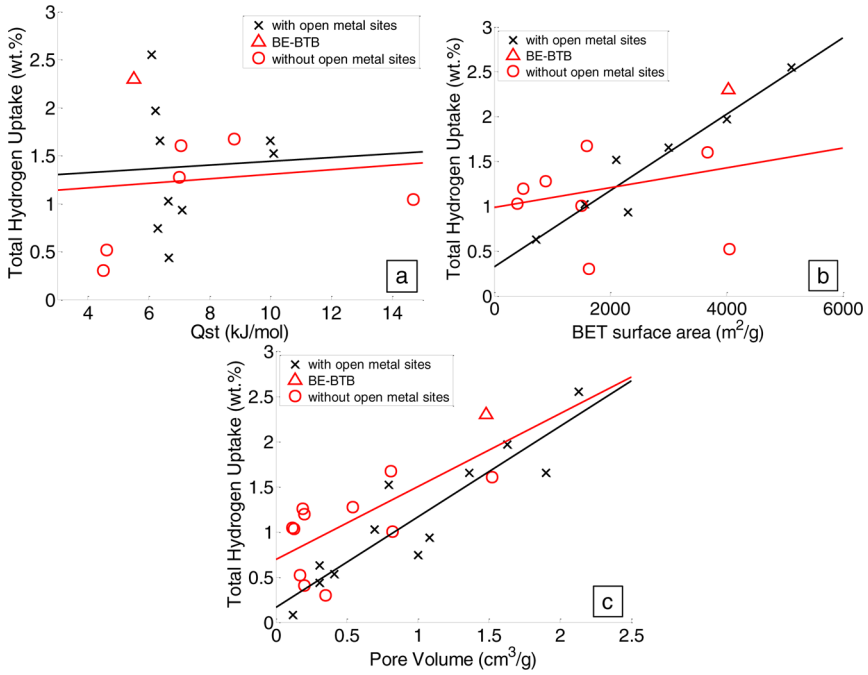

Figure 2. Total H_2 uptake at room temperature and high pressures (more than 35 bar). Data other than Be-BTB are taken from Suh et al.[4] (a) H_2 uptake versus heat of adsorption; (b) H_2 uptake versus BET surface area; (c) H_2 uptake versus pore volume. The R^2 value for MOFs with and without open metal sites are 0.23% and 1.43% for (a), 90.99% and 7.22% for (b), and 83.43% and 52.63% for (c).

Table 1. Coefficient of Determination (R^2) for the Correlation of Total H_2 Uptake with Heat of Adsorption (Q), BET Surface Area (BET), and Pore Volume (PV)

variables	with open metal sites (%)	without open metal sites (%)
Q	0.23	1.43
BET	90.99	7.22
PV	83.43	52.63

surface area and bond enthalpy to room temperature performance, and to examine the pore architecture within Be-BTB to understand its role in both hydrogen storage and cyclability.

2. MODELING METHODOLOGY

When the H_2 gas is inside the Be-BTB framework, it is acted upon by intermolecular van der Waals forces with every atom comprising the Be-BTB. This phenomenon may be accurately modeled using the 6-12 Lennard–Jones potential function[20] where the intermolecular potential energy between two nonbonded atoms of interest (framework atom and H_2 molecule) is given by

$$\Phi(\rho) = 4\varepsilon\left[-\left(\frac{\sigma}{\rho}\right)^6 + \left(\frac{\sigma}{\rho}\right)^{12}\right] \quad (1)$$

where ρ is the distance between the atoms, σ is the atomic distance when the potential energy is zero, and ε is the value of the energy when the atoms are at the equilibrium distance, $\rho_0 = 2^{1/6}\sigma$. The negative and positive terms in eq 1 describe the balance of attractive and repulsive forces experienced by the two atoms of interest. The interatomic potential parameters for a different species of atoms (σ and ε) are determined using the empirical Lorentz–Berthelot mixing rules where $\varepsilon_{12} = (\varepsilon_1\varepsilon_2)^{1/2}$ and $\sigma_{12} = (\sigma_1 + \sigma_2)/2$. The long-range electrostatic forces which also contribute to the atomic interaction are found to have negligible effects on the total hydrogen uptake.[7] The parameter values for the framework atoms and a H_2 gas molecule are given in Table S3.

In this work, we use two methods to predict the H_2 adsorption within the Be-BTB framework: a numerical atomistic simulation approach and an analytic Topologically Integrated Mathematical Thermodynamic Adsorption Model (TIMTAM).[21] The atomistic simulation approach offers specific insight into the exact location of H_2 adsorption within the MOF, while the analytical TIMTAM approach offers immediate access to the complete isotherm profiles for any temperature and pressure. The latter approach is compatible with the TEO routine utilized here to determine the feasibility of MOFs in a fuel cell application in comparison to a compressed gas tank.

2.1. Atomistic Simulation Details. The atomistic simulation of Be-BTB is constructed according to the fixed atomic coordinates determined by Sumida et al.[15] To predict the equilibrium H_2 adsorption within the framework, the Grand Canonical Monte Carlo (GCMC) algorithm[22] is implemented with the RASPA software package.[23] Force fields for the framework are taken from the universal force field (UFF)[24] while H_2 is treated as a single-site model according to van den Berg et al.[25] Force field cutoffs of 12.8 Å are implemented. More details are found in the Supporting Information. The GCMC algorithm trials a series of random H_2 moves including addition, deletion, rotation, and translation. The probability of accepting each move is based upon the Grand Canonical ensemble relating the specific temperature, volume, and chemical potential. 1 000 000 equilibration steps are followed by 100 000 production steps. The final ensemble represents a statistical average of the equilibrium states. Complete isotherms are produced up to 100 bar for temperatures 77 and 298 K.

2.2. TIMTAM Formulation. The TIMTAM approach[21] uses applied mathematical modeling to represent the structure of Be-BTB with assumed ideal building blocks that comprise continuous surfaces and volumes for adsorption. TIMTAM is a phenomenological model based on approximations that have proved useful in investigating the effect of pore size.[21,26] Figure 3 shows the Be-BTB structure as an ideal composition of cylindrical rings, which represent the $[Be_{12}(OH)_{12}]^{12+}$ rings (or Be-ring), and spheres which represents the connected BTB^{3-} ligands comprised mostly of carbon and hydrogen atoms. At first sight such a simplified modeling approach may seem geometrically severe, but in similar situations it has been shown to provide the major contribution to the interaction energy of the actual structure, confirmed by either independent experimental results or computa-

dx.doi.org/10.1021/la401446s | Langmuir 2013, 29, 8524–8533

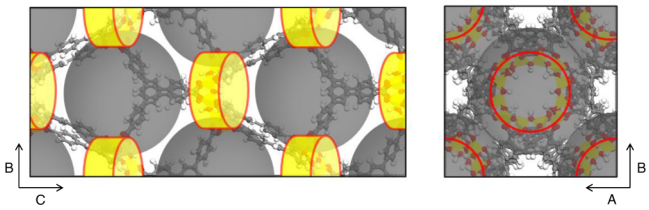

Figure 3. Structure of Be-BTB. Spheres and cylinders represent ideal building blocks for adsorption cavities in the structure.

tional modeling.[21,27,28] Calculations that involves the TIMTAM approach are evaluated using the algebraic computer package MAPLE.

In principle, the total potential energy within the system, $U_{tot}(\rho)$, is obtained by a summation of the potential energy for the interaction between H_2 and an infinite cylindrical ring with the potential energy for the interaction between H_2 and a sphere. The potential energy for an infinite cylinder interacting with the H_2 molecule based on the model by Cox et al.[27] and Thornton et al.[21] is given by

$$U_1(\rho) = \sum_{i=1}^{3} \eta_i(-A_iR_3 + B_iR_6)$$

$$R_j = \frac{8\pi^2 r_1^2}{(2r_1)^{2j}(2j-2)!} \sum_{s=1}^{\infty} \left[\frac{\rho^s(2j+2s-2)!}{(4r_1)^s s!(j+s-1)!}\right]^2 \quad (2)$$

where ρ is the distance between the H_2 molecule and the center of the cavity; η_i denotes the mean atomic surface densities of atom i on the cavity surface at radius r_1. To make the mathematics tractable, we assume that the interaction is accurately approximated by the potential energy of an infinite cylinder. However, when determining the gravimetric uptake, the volume of the cylinder is calculated by multiplying the length of the actual beryllium-ring (Be-ring), h, by the area of the base, $2\pi r_1$. The potential energy within a sphere of radius r_2, based on the model by Cox et al.[29] and Thornton et al.,[21] is given by the expression

$$U_2(\rho) = \sum_{j=2}^{4} \eta_j(-A_jQ_6 + B_jQ_{12})$$

$$Q_k = \frac{2r_2\pi}{\rho(2-k)}\left[\frac{1}{(\rho+r_2)^{k-2}} - \frac{1}{(\rho-r_2)^{k-2}}\right] \quad (3)$$

Based on the paper by Walton and Snurr,[30] adsorption in MOFs can be dominated by the pore filling or multilayered formation mechanism. To ensure that both types of adsorption are considered in our model, we make assumptions that the gas molecule can exist as a mixture of adsorbed and bulk gas in the MOF structure. The probability that the molecule is adsorbed on the surface of the cavity can be expressed as $1 - \exp(U/RT)$ when its potential energy (U) is larger than its kinetic energy, represented by RT, the ideal gas constant (R) and the temperature (T). Consequently, the probability that the molecule exists as bulk gas phase is $\exp(U/RT)$. In this formulation, pore filling and multilayer mechanisms are not distinguishable, although the ratio of bulk phase over adsorbed phase is an approximate indicator.

As indicated in the Introduction, free volume (or pore volume) is a property worthy of exploration for its role in adsorbent performance. Total free volume (V_f) comprises the volume available for adsorbed phase (V_{ad}) and the volume available for bulk gas phase that remains within each of the ideal building blocks (V_{bulk}). Within the Be-ring and sphere, V_{ad} is calculated by integrating the probability of adsorption over the total free volume, and V_{bulk} is calculated by integrating the probability that the molecule remains as bulk gas over the total free volume. The formulas for V_{ad} and V_{bulk} for the Be-ring are given by

$$V_{ad} = \int_0^{\rho_1} 2\pi\rho h\left(1 - \exp\left[\frac{U}{RT}\right]\right) d\rho$$

$$V_{bulk} = \int_0^{\rho_1} 2\pi\rho h\left(\exp\left[\frac{U}{RT}\right]\right) d\rho \quad (4)$$

and the formulas for the sphere are given by

$$V_{ad} = \int_0^{\rho_2} 4\pi\rho^2\left(1 - \exp\left[\frac{U}{RT}\right]\right) d\rho$$

$$V_{bulk} = \int_0^{\rho_2} 4\pi\rho^2\left(\exp\left[\frac{U}{RT}\right]\right) d\rho \quad (5)$$

where h is the height of the cylinder, ρ_1 is the radial boundary of the free volume, and ρ_2 is the value of the radius where potential is zero for the cylinder and sphere.[26] The radius of the Be-ring is measured from the atomistic structure, and the radius of the sphere is adjusted such that the total free volume matched that found in the atomistic cell.

The total number of H_2 molecules in the cavity is approximated by combining V_{ad} and V_{bulk} with the appropriate equation of state. The number of molecules in bulk gas state (n_{bulk}) is obtained by solving the simplified van der Waals equation of state to obtain

$$P\left(\frac{V_{bulk}}{n_{bulk}} - C\right) = RT, \quad C = \frac{RT_c}{8P_c} \quad (6)$$

where P is the pressure and C is the occupied volume calculated from the critical temperature T_c and critical pressure P_c for H_2. The number of molecules in the adsorbed phase (n_{ad}) is calculated by solving a modified version of the Dieterici equation of state to obtain

$$P\left(\frac{V_{ad}}{n_{ad}} - C\right) = RT\exp\left(\frac{-Q}{RT}\right) \quad (7)$$

where Q is the heat of adsorption described by Everett and Powl[31] as

$$Q = |U_{min}| + \alpha RT \quad (8)$$

where U_{min} is the minimum potential energy (i.e., the strongest well for capturing H_2) and α represents the excess thermal energy in the adsorbed phase, fixed at 0.5.[31] The α constant may vary for different materials, and therefore, the model should be used as an insightful fit rather than a complete prediction. By rearrangement, eq 7 is identical to the Boltzmann distribution law where local density is proportional to $\exp(-U/kT)$.[32,33] The total gravimetric uptake is determined using the total number of molecules, $n = n_{ad} + n_{bulk}$, as follows

$$H_2 \text{ uptake (wt \%)} = \frac{nm}{nm + M} \times 100 \quad (9)$$

where m is the mass of a hydrogen molecule and M is the mass of a unit cell of the Be-BTB cavity. The parameter values used to calculate the number of molecules and total adsorption are given in Table S4 in the Supporting Information.

2.3. Thermodynamic Energy Optimization of Operating Conditions. The optimum storage and delivery condition for a H_2 fuel cell based on MOFs can be determined using the thermodynamic energy optimization (TEO) model. The TEO model used to determine the total energy generated from the fuel cell is based on the work of Lin et al.[34] who present a method used to optimize the regeneration conditions for materials utilized for carbon dioxide capture and storage using a combined temperature-swing pressure-swing process. This optimization is achieved by minimizing the electric load imposed on a power plant. The electric load depends on three types of energy: energy required to (i) heat the material, (ii) supply the heat of desorption (equivalent to the heat of adsorption), and (iii) pressurize the gas to the standard transport and storage pressure.

Here we aim to calculate the optimal storage and delivery conditions for a H_2 fuel cell concentrating only on the energy produced by pressure and/or temperature swing adsorption cycle, ignoring any other factors such as insulation, tank mass, and heaters.

dx.doi.org/10.1021/la401446s | Langmuir 2013, 29, 8524−8533

Hence, the total energy generated from H_2 stored in the fuel cell is given by

$$E_{tot} = E_{fc}W_c - V|P_{ads} - P_{des}| - C_p|T_{ads} - T_{des}| - QW_c \quad (10)$$

$$W_c = n_{ads} - n_{des} \quad (11)$$

where the subscript ads denotes storage condition and des denotes delivery condition. The first term in eq 10 calculates the total energy produced by the fuel cell where E_{fc} is the amount of energy per mole of hydrogen which can be provided as electrical energy (calculated to be 237.1 kJ mol^{-1} using the Gibbs free energy function[35]) and W_c is the working capacity of the material, which is the difference in amount of H_2 adsorbed at pressure P_{ads} and P_{des} and temperature T_{ads} and T_{des}. The second term determines the energy required to increase the pressure, and the third term determines the energy required to heat the material from storage condition to desorption condition. Finally, the last term represents the energy required to remove a mol of gas. V denotes the volume of a unit cell of adsorbant, and C_p and Q are the specific heat capacity and heat of adsorption of the adsorbant, respectively. The parameter values are listed in Table S5 of the Supporting Information.

3. RESULTS AND DISCUSSION

To ensure that the atomistic simulation and the mathematical modeling approaches describe the properties of the Be-BTB structure accurately, the gravimetric uptake at 77 and 298 K is compared to the experimental data.[15] The experimental data has been converted from excess to total uptake using the method outlined by Frost and Snurr.[16] Total uptake is of interest here for the DOE requirements and comparison with compressed tank.[36] See Figure S1 for comparison with excess uptake.

The GCMC simulation and TIMTAM continuum modeling results are shown to be in good agreement with the experimental results in Figure 4. For the 77 K data, remarkably

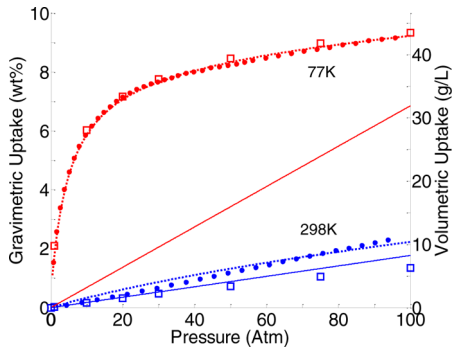

Figure 4. Total H_2 uptake at 77 and 298 K for model and experimental data.[15] Solid lines show the density of compressed H_2 gas in a tank at 77 and 298 K. Circles represent experimental data, squares represent GCMC model results, and dotted lines represent TIMTAM predictions for Be-BTB.

the Be-BTB stores up to four times more H_2 than the compressed gas tank (solid lines). At room temperature, the GCMC results slightly underestimate the experimental uptake, possibly due to interaction energy cutoffs chosen for efficient computation resulting in close to compressed gas phase.

As shown in Figure 1, the atomistic simulation reveals no specific adsorption sites of H_2 within the framework. There is a relatively uniform distribution of H_2 with only a slight preference toward the Be-ring building block. Even without strong binding sites, the overall H_2 adsorption within Be-BTB surpasses that of H_2 in a compressed gas tank. More importantly, the TIMTAM approach accurately describes the isotherm profiles that we will analyze later with the TEO model.

3.1. Pore Size Analysis. The pore size distribution (PSD) is a critical property to examine because the strength of adsorption of gases onto the structure varies with the size of the pores.[37] To compute the pore size distribution, we utilize two approaches: (i) a geometrical approach (GA) explained by Gelb and Gubbins[38] implemented through the software package RASPA,[23] and (ii) an energetic approach, namely, the Cavity Energetic Sizing Algorithm (CESA), reported by Wang et al.[39]

CESA focuses on the pores with a distinct energy environment while GA is purely geometric, ignoring any energetic considerations. Both methods operate on the atomistic representation shown in Figure 3. The experimental PSD by Sumida et al.[15] was calculated from argon adsorption data using nonlocal density functional theory (NFDFT) and a hybrid kernel based on a zeolite/silica cylindrical pore model. Both the energetic and geometric sizing algorithms assume nothing about the pore geometry but assume spherical probe geometry. There is excellent agreement between the experimental and simulated PSD even though the NLDFT does not consider gas−MOF interactions. A possible explanation is that the argon_-MOF and argon−zeolite/silica interactions are similar.

The PSD from experimental nitrogen adsorption results[15] is compared to the computational results in Figure 5. The

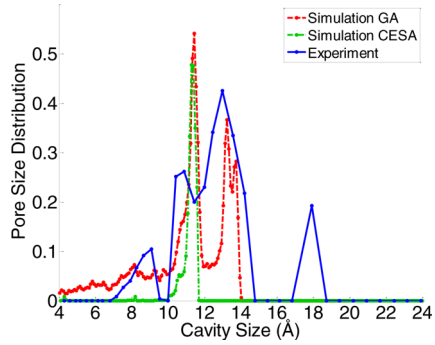

Figure 5. Pore size distribution obtained from experimental nitrogen adsorption data by Sumida et al.[15] and computational results from the GA and the CESA.

experimental data indicate that there is a broad PSD with peaks at ~8, 11, 13, and 18 Å. The GA simulation predicts peaks at ~8, 11, and 13 Å. The CESA method predicts a peak at 11 Å only. The experimental PSD peak at 18 Å is most likely due to interparticle pores. The CESA method emphasizes the dominant pore size that is energetically favorable, ~ 11 Å, which is close to the Be-ring cavity size of 9 Å. As a H_2 molecule has a diameter of 2.958 Å, a pore size of ≥9 Å will allow for confined adsorption in the cavity which is an ideal scenario.[40]

To explore the importance of the Be-ring cavity, the potential energy within the ring and sphere building blocks is analyzed using TIMTAM and displayed in Figure 6. The H_2 interaction with the Be-ring has a deeper potential energy minimum compared to the spherical cavity; therefore, the gas experiences a stronger interaction with the Be-ring compared to the spherical cavity of the Be-BTB. Thus, as H_2 is adsorbed into Be-BTB, it will first prefer to be adsorbed at the minimum

dx.doi.org/10.1021/la401446s | Langmuir 2013, 29, 8524−8533

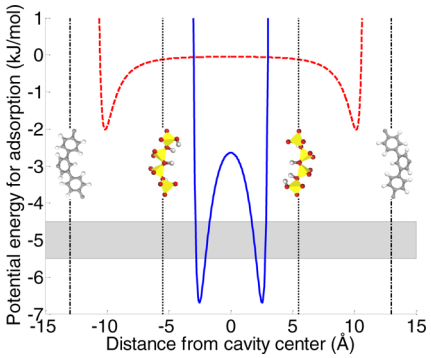

Figure 6. Potential energy for the ideal Be-BTB building blocks of BTB^{3-} spherical cavities (red dashed line) and cylindrical Be-ring cavities (blue solid line) that were constructed for the TIMTAM approximation. Shaded area represents heat of adsorption measured experimentally.[15]

potential energy of the Be-ring at a distance of 2.6 Å from the center of the Be-ring cavity, after which it will start to adsorb onto the surface of the spherical cavity at a distance of 10 Å from the center of the spherical cavity. Further analysis shows that the heat of adsorption for the Be-ring is predicted to be 4.8 kJ mol^{-1}, which is consistent with the measured heat of adsorption reported as 4.5−5.5 kJ mol^{-1}.[15]

3.2. Fractional Free Volume. To understand the effect of the pore size on the adsorption capacity of the Be-BTB, a fractional free volume analysis is done for the Be-ring cavity at 77 and 298 K. The fractional free volume for adsorption describes the proportion of volume of H_2 gas in the cavity that is in the adsorbed state as compared to bulk gaseous state (V_{ad}/V). This quantity is shown in Figure 7 and indicates that at 298

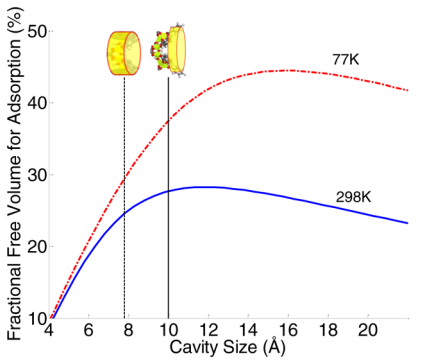

Figure 7. Fractional free volume for adsorption (V_{ad}/V) at 77 and 298 K within the Be-ring cylindrical cavity building block.

K the 9 Å size of the Be-ring cylindrical cavity and its surrounding configuration is very close to the optimal size. Up to 23% of the free volume within the Be-ring cavity is able to store H_2 gas in its adsorbed state. At 77 K, gas adsorption is at optimum level when the effective pore size is 15 Å due to the decreased importance of kinetic energy over interatomic potential energy. A larger cavity size allows more gas molecules to be adsorbed at larger distances and therefore encourages multiple adsorption layers.

The study by Wang and Johnson[41] which investigated the adsorption capabilities of carbon slit pores and carbon nanotubes indicated that the density of hydrogen is not liquidlike at room temperature. Thus, the amount of adsorbed H_2 is usually smaller than the amount of bulk H_2 gas at room temperature. A similar relationship can be observed in Figure 7 which shows that the fractional free volume for adsorption at room temperature is lower than that at 77 K inside the cylindrical Be-ring cavity of Be-BTB. The effects of van der Waals interaction on H_2 is therefore less pronounced at room temperature than at 77 K.

3.3. Optimal Storage and Delivery Conditions. In this section, the optimal cycle conditions for a Be-BTB fuel cell are compared to a MOF-5 fuel cell, a MOF-177 fuel cell and a compressed H_2 tank fuel cell, concentrating only on the pressure and/or temperature adsorption process and ignoring other factors that contribute to the production of energy.

The energy produced by these fuel cells is analyzed using the TEO optimization function. This function optimizes the operating pressure and temperature within the range of delivery pressure of 5−12 bar, and delivery and operating temperatures of 233−358 and 233−333 K, respectively, as set by the 2017 U.S. DOE target.[1] The adsorption pressure is set to 100 bar for pressure−swing (Tables 2 and 4) and 12 bar for temperature-swing (Table 3) so that the systems can be compared effectively.

Table 2. Maximum Energy Generation at Optimized Storage (ads) and Delivery (des) Conditions Restricted to DOE Operating Range for a Pressure−Swing Only Cycle

parameter	tank[a]	MOF-5	Be-BTB	MOF-177
P_{ads} (bar)	100	100	100	100
P_{des} (bar)	5	5	5	5
T_{ads} (K)	233	233	233	233
T_{des} (K)	233	233	233	233
E_{tot} (kW h/L)	0.35	0.07	0.32	0.24
E_{tot} (kW h/kg)	34.93	0.12	0.75	0.57

[a]Compressed H_2 gas.

Table 3. Maximum Energy Generation at Optimized Storage (ads) and Delivery (des) Conditions Restricted to the DOE Operating Range for a Temperature−Swing Only Cycle

parameter	tank[a]	MOF-5	Be-BTB	MOF-177
P_{ads} (bar)	12	12	12	12
P_{des} (bar)	12	12	12	12
T_{ads} (K)	233	233	233	233
T_{des} (K)	302	358	358	358
E_{tot} (kW h/L)	0.01	0.004	0.04	0.01
E_{tot} (kW h/kg)	35.21	0.007	0.10	0.02

[a]Compressed H_2 gas.

A study on densified MOF-177 pellets by Dailly and Poirier[42] revealed a decrease in available pore volume of around 24% compaed with the known crystal pore volume. To account for this occurrence in our calculations, the hydrogen uptake is decreased by 24%. We would like to note here that total gravimetric uptake is considered instead of excess gravimetric uptake to allow for comparison with the 2017 U.S. DOE targets which uses total gravimetric uptake.

The number of H_2 molecules at varying pressures and temperatures for Be-BTB and MOF-5 are calculated using the TIMTAM model described in eqs 2−7. The TIMTAM parameters for MOF-5 are obtained from Thornton et al.[26] For MOF-177, the number of H_2 molecules at varying pressures and temperatures have been calculated from the modified Dubinin-Astakhov model[43] using the fitted parame-

dx.doi.org/10.1021/la401446s | Langmuir 2013, 29, 8524−8533

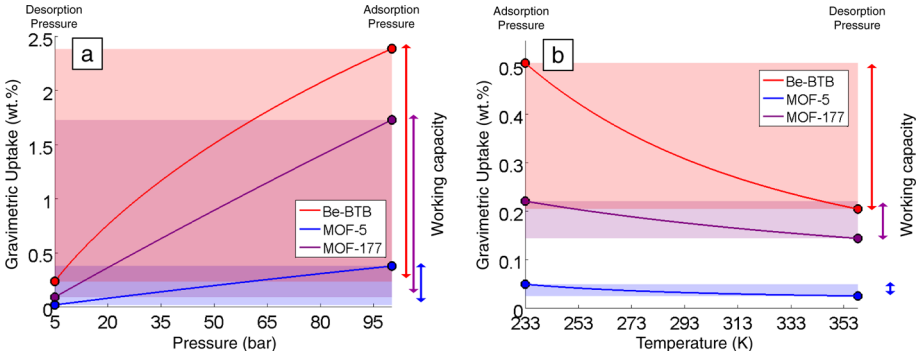

Figure 8. (a) Optimum gravimetric H_2 uptake at 233 K for a pressure−swing adsorption process. (b) Optimum gravimetric H_2 uptake at 12 bar for a temperature−swing adsorption process.

ters from Poirier and Dailly.[44] The number of H_2 molecules in a compressed gas tank is calculated using the ideal gas law matching the standard for engineering assessments.[45]

3.3.1. Pressure−Swing Adsorption Cycle. A pressure−swing only adsorption cycle is considered where the operating temperature is fixed to the DOE fuel cell standards. Results of this analysis are reported in Table 2, which shows that the H_2 tank is the most efficient at producing energy compared to the MOF-based fuel cells, particularly for energy per mass at 34.93 kWh/kg. Among the MOF-based fuel cells, Be-BTB produces the most energy per mass and volume, followed by MOF-177 and MOF-5. Our calculations show that 233 K is the optimum temperature for the pressure−swing for all three MOF-based fuel cells, with adsorption pressure of 100 bar and desorption pressure of 5 bar.

Figure 8a provides a visual comparison of their optimal working capacities for a pressure−swing only process utilizing Be-BTB, MOF-5, or MOF-177. A Be-BTB fuel cell clearly outperforms the other MOF-based fuel cells because of the higher gravimetric and volumetric uptake at all pressures. In addition, a Be-BTB fuel cell has the largest working capacity (as shown by the red arrow to the right of the figure), followed by a MOF-177 (purple arrow) and MOF-5 (blue arrow) fuel cell.

3.3.2. Temperature−Swing Adsorption Cycle. Analysis for a temperature−swing only adsorption process for the compressed gas tank and MOF-based fuel cells show that the optimum operating pressure for a temperature−swing fuel cell is 12 bar and adsorption temperature of 233 K. The optimum desorption temperature is 302 K for a H_2 tank and 358 K for MOF-5, Be-BTB, and MOF-177.

The analysis from the TEO model which is presented in Table 3 shows that the Be-BTB fuel cell produces the most energy per volume followed by the H_2 tank and MOF-177 (both at 0.01 kWh/L) and last by a MOF-5 fuel cell. The H_2 tank produces the most energy per mass at 35.21 kWh/kg. Among the MOF-based fuel cells, Be-BTB produces the most energy per mass, followed by MOF-177 and MOF-5.

Figure 8b provides a visual comparison between the three MOFs for the temperature-swing only cycle. It can be observed that Be-BTB has the highest gravimetric and volumetric uptake at all temperatures between 233 - 358 K, followed by MOF-177 and MOF-5. In addition, Be-BTB (denoted by the red arrow to the right of the figure) has the largest range of working capacity, followed by MOF-177 (purple arrow) and MOF-5 (blue arrow). Comparisons between Figure 8a and b shows that the pressure−swing adsorption process produces more energy compared to the temperature-swing adsorption process due to the larger working capacity.

3.3.3. Combined Pressure and Temperature−Swing Cycle. The optimum desorption pressure and adsorption temperature are calculated to be 5 bar and 233 K for all four systems when analyzing a combined pressure−swing and temperature−swing adsorption process. Our analysis presented in Table 4 shows that the H_2 tank produces the most energy compared to the MOF-based fuel cells, particularly for energy per mass at 34.9 kW h/kg. Among the MOF-based fuel cells, Be-BTB produces the most energy for both mass and volume, followed by MOF-177 and MOF-5.

Table 4. Maximum Energy Generation at Optimized Storage (ads) and Delivery (des) Conditions Restricted to the DOE Operating Range for a Combined Pressure−Swing and Temperature−Swing Cycle

parameter	tank[a]	MOF-5	Be-BTB	MOF-177
P_{ads} (bar)	100	100	100	100
P_{des} (bar)	5	5	5	5
T_{ads} (K)	233	233	233	233
T_{des} (K)	302	358	358	358
E_{tot} (kW h/L)	0.35	0.07	0.34	0.25
E_{tot} (kW h/kg)	34.93	0.12	0.80	0.58

[a]Compressed H_2 gas.

Figure 9 displays the contour plots of the gravimetric uptake of Be-BTB, MOF-5, and MOF-177 with respect to temperature and pressure at the standard operating conditions. The contour plots show that the gas uptake for a Be-BTB fuel cell is higher than that of MOF-5 and MOF-177 at any combination of temperature and pressure.

Overall, when limited by the U.S DOE operating pressure and temperature, the H_2 tank produces substantially more energy per mass for all three types of adsorption processes compared to the MOF-based fuel cells. The H_2 tank also produces more energy per volume except for the temperature-swing only cycle where the Be-BTB fuel cell has a higher energy output. Among the MOF-based fuel cells, the Be-BTB fuel cell generates the most energy per volume and mass, followed by MOF-177 and MOF-5.

The 2017 U.S. DOE target for energy produced by onboard H_2 storage systems is 1.3 kW h/L for volumetric capacity and 1.8 kW h/kg for gravimetric capacity. Our results show that only a compressed gas tank satisfy the U.S. DOE requirement for the gravimetric capacity. The H_2 tank does not satisfy the

dx.doi.org/10.1021/la401446s | Langmuir 2013, 29, 8524−8533

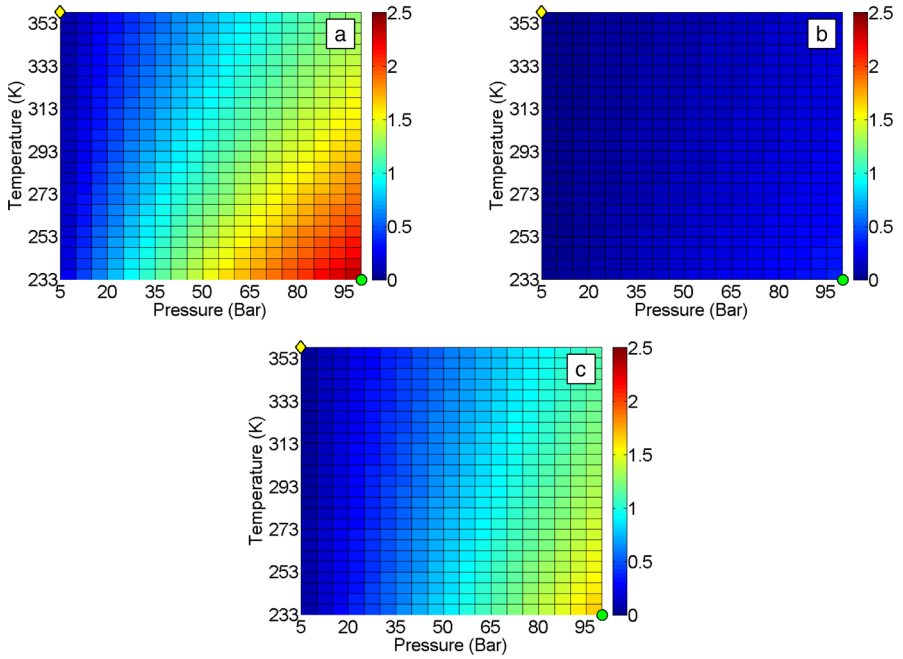

Figure 9. H_2 gravimetric uptake with respect to temperature and pressure. (a) H_2 uptake for Be-BTB. (b) H_2 uptake for MOF-5. (c) H_2 uptake for MOF-177. The yellow cross and green circle denote the TEO optimized desorption and adsorption conditions, respectively, that maximizes the net energy. The bar on the right describes the value gravimetric uptake in wt %.

requirements for the volumetric capacity, and the MOF-based fuel cells also do not reach the standard of requirements for both the gravimetric and volumetric capacities for any of the adsorption processes. Overall, there is still much improvement in MOF performance required to meet the DOE targets.

4. CONCLUSIONS

We model the adsorption of H_2 by Be-BTB utilizing atomistic simulation and continuum modeling using ideal building block representations of the surfaces and volumes of adsorption. The atomistic simulation confirms that the model Be-BTB structure replicates the experimental H_2 uptake. The continuum model allows exploration of the available parameter landscape for optimizing H_2 uptake. Our calculations using the TIMTAM model show that a H_2 molecule experiences a stronger interaction with the Be-ring cavity as compared to the spherical cavity of the Be-BTB. At 298 K, the size of the Be-ring cavity, 9 Å, is at the optimum size to encourage efficient adsorption of gas.

Comparisons of Be-BTB with MOFs with and without open metal sites confirm the findings of Frost et al.[7] that the uptake of H_2 is correlated with pore volume for weak adsorption (MOFs without metal sites), and surface area and pore volume for stronger adsorption (MOFs with metal sites) at room temperature. We also analyze and compare the energy output from H_2 compressed in a gas tank and adsorbed H_2 in MOF-based fuel cells. To do this, we performed the thermodynamic energy optimization (TEO) model which is based on the Gibbs free energy function[35] and the working capacity of the MOF[34] using three different adsorption processes: (i) pressure−swing only, (ii) temperature−swing only, and the (iii) combined pressure and temperature−swing process.

Our results show that an adsorption process that relies on the three aforementioned processes is not enough for the compressed tank and MOF-based fuel cells to achieve the 2017 U.S. DOE volumetric capacity target of 1.3 kW h/L. For the gravimetric capacity, only the compressed tank fulfills the U.S. DOE gravimetric capacity of 1.8 kW h/kg. Among the MOF-based fuel cells, the Be-BTB fuel cell provides the most energy per volume and per mass, followed by MOF-177 and MOF-5. We attribute this to the superior pore effect which the Be-BTB has over MOF-5 and MOF-177. Our analysis using the TEO model shows that there is still much improvement in MOF performance required to meet the DOE targets.

■ ASSOCIATED CONTENT

Ⓢ Supporting Information

Full details of parameters used for our calculations and data for H_2 for MOFs with and without open metal sites. This material is available free of charge via the Internet at http://pubs.acs.org/.

■ AUTHOR INFORMATION

Corresponding Author

*E-mail: aaron.thornton@csiro.au.

Notes

The authors declare no competing financial interest.

■ ACKNOWLEDGMENTS

W.-X.L., A.W.T., A.J.H., and M.R.H. acknowledge the support of the Computational and Simulation Science Transformational Capability Platform and the Office of the Chief Executive Science Team at CSIRO. B.J.C. and J.M.H. acknowledge the support of the Australian Research Council through the Discovery Projects scheme. The authors also acknowledge the facilities and services provided through the CSIRO Accelerated Scientific Computing.

■ REFERENCES

(1) United States Department of Energy. Targets for Onboard Hydrogen Storage Systems for Light-Duty Vehicles, 2009; http://

www1.eere.energy.gov/hydrogenandfuelcells/storage/pdfs/targets_onboard_hydro_storage_explanation.pdf (accessed Sept 20, 2012).
(2) Schlapbach, L.; Züttel, A. Hydrogen Storage Materials forMobile Applications. *Nature* **2001**, *414*, 353−358.
(3) Hydrogen Storage Summary of Annual Merit Review of the Hydrogen Storage Sub-Program, 2012; http://www.hydrogen.energy.gov/pdfs/review12/55568-04_storage.pdf.
(4) Suh, M. P.; Park, H. J.; Prasad, T. K.; Lim, D.-W. Hydrogen Storage in Metal-Organic Frameworks. *Chem. Rev.* **2012**, *112*, 782−835.
(5) Bhatia, S. K.; Myers, A. L. Optimum Conditions for Adsorptive Storage. *Langmuir* **2006**, *22*, 1688−1700.
(6) Düren, T.; Millange, F.; Ferey, G.; Walton, K. S.; Snurr, R. Q. Calculating Geometric Surface Areas as a Characterization Tool for Metal-Organic Frameworks. *J. Phys. Chem. C* **2007**, *111*, 15350−15356.
(7) Frost, H.; Düren, T.; Snurr, R. Q. Effects of Surface Area, Free Volume, and Heat of Adsorption on Hydrogen Uptake in Metal-Organic Frameworks. *J. Phys. Chem. B* **2006**, *110*, 9565−70.
(8) Rowsell, J. L. C.; Yaghi, O. M. Metal-Organic Drameworks: A New Class of Porous Materials. *Microporous Mesoporous Mater.* **2004**, *73*, 3−14.
(9) Kubas, G. J. Fundamentals of H_2 Binding and Reactivity on Transition Metals Underlying Hydrogenase Function and H_2 Production and Storage. *Chem. Rev.* **2007**, *107*, 4152−4205.
(10) Schnobrich, J. K.; Koh, K.; Sura, K. N.; Matzger, A. J. AFramework for Predicting Surface Areas in Microporous Coordination Polymers. *Langmuir* **2010**, *26*, 5808−5814.
(11) Lin, X.; Jia, J.; Zhao, X.; Thomas, K. M.; Blake, A. J.; Walker, G. S.; Champness, N. R.; Hubberstey, P.; Schröder, M. High H_2 Adsorption by Coordination-Framework Materials. *Angew. Chem., Int. Ed.* **2006**, *45*, 7358−7364.
(12) Watanabe, T.; Sholl, D. S. Accelerating Applications of Metal-Organic Frameworks for Gas Adsorption and Separation by Computational Screening of Materials. *Langmuir* **2012**, *28*, 14114−14128.
(13) Furukawa, H.; Ko, N.; Go, Y. B.; Aratani, N.; Choi, S. B.; Choi, E.; Yazaydin, A. Ö.; Snurr, R. Q.; O'Keeffe, M.; Kim, J.; Yaghi, O. M. Ultra-High Porosity in Metal-Organic Frameworks. *Science* **2010**, *424*, 2159−2171.
(14) Brunauer, S.; Emmett, P. H.; Teller, E. Adsorption of Gases in Multimolecular Layers. *J. Am. Chem. Soc.* **1938**, *60*, 309−319.
(15) Sumida, K.; Hill, M. R.; Hiroke, S.; Dailly, A.; Long, J. R.Synthesis and Hydrogen Storage Properties of $Be_{12}(OH)_{12}$(1,3,5-benzenetribenzoate)$_4$. *J. Am. Chem. Soc.* **2009**, *131*, 15120−15121.
(16) Frost, H.; Snurr, R. Q. Design Requirements for Metal-Organic Frameworks as Hydrogen Storage Materials. *J. Phys. Chem. C* **2007**, *111*, 18794−18803.
(17) Yazaydin, A. Ö.; Snurr, R. Q.; Park, T.-H.; Koh, K.; Liu, J.; LeVan, M. D.; Benin, A. I.; Jakubczak, P.; Lanuza, M.; Galloway, D. B.; Low, J. J.; Willis, R. R. Screening of Metal-Organic Frameworks for Carbon Dioxide Capture from Flue Gas Using a Combined Experimental and Modelling Approach. *J. Am. Chem. Soc.* **2009**, *131*, 18198−18199.
(18) Team, R. C. R A Language and Environment for Statistical Computing. R Foundation for Statistical Computing: Vienna, Austria, 2012; ISBN 3-900051-07-0.
(19) Porter, W. W.; Wong-Foy, A.; Dailly, A.; Matzger, A. J. Beryllium Benzene Dicarboxylate: The First Beryllium Microporous Coordination Polymer. *J. Mater. Chem.* **2009**, *19*, 6489−6491.
(20) Lennard-Jones, J. E. Cohesion. *Proc. Phys. Soc.* **1931**, *43*, 461−482.
(21) Thornton, A. W.; Furman, S. A.; Nairn, K. M.; Hill, A. J.; Hill, J. M.; Hill, M. R. Analytical Representation of Micropores for Predicting Gas Adsorption in Porous Materials. *Microporous Mesoporous Mater.* **2013**, *167*, 188−197.
(22) Snurr, R. Q.; Bell, A. T.; Theodorou, D. N. Prediction of Adsorption of Aromatic Hydrocarbons in Silicalite from Grand Canonical Monte Carlo Simulations with Biased Insertions. *J. Phys. Chem.* **1993**, *97*, 13742−13752.
(23) Dubbeldam, D.; Calero, S.; Ellis, D. E.; Snurr, R. Q. *RASPA*, version 1.0; Northwestern University: Evanston IL, 2008.
(24) Rappe, A. K.; Casewit, C. J.; Colwell, K. S.; Goddard, W. A.; Skiff, W. M.; UFF, A. Full Periodic Table Force Field for Molecular Mechanics and Molecular Dynamics Simulations. *J. Am. Chem. Soc.* **1992**, *114*, 10024−10035.
(25) van den Berg, A. W. C.; Bromley, S. T.; Wojdel, J. C.; Jansen, J. C. Adsorption Isotherms of H_2 in Microporous Materials with the SOD Structure: A Grand Canonical Monte Carlo Study. *Microporous Mesoporous Mater.* **2006**, *87*, 235−242.
(26) Thornton, A. W.; Nairn, K. M.; Hill, J. M.; Hill, A. J.; Hill, M. R. Metal-Organic Frameworks Impregnated with Magnesium-Decorated Fullerenes for Methane and Hydrogen Storage. *J. Am. Chem. Soc.* **2009**, *131*, 10662−10669.
(27) Cox, B. J.; Thamwattana, N.; Hill, J. M. Orientation of Spheroidal Fullerenes Inside Carbon Nanotubes with Potential Applications as Memory Devices in Nano-Computing. *J. Phys. A: Math. Theor.* **2008**, *41*, 1−27.
(28) Chan, Y.; Hill, J. M. Hydrogen Storage inside Graphene-Oxide Frameworks. *Nanotechnology* **2011**, *22*, 1−8.
(29) Cox, B. J.; Thamwattana, N.; Hill, J. M. Mechanics of Atoms and Fullerenes in Single-Walled Carbon Nanotubes. I. Acceptance and Suction Energies. *Proc. R. Soc. A* **2007**, *463*, 461−477.
(30) Walton, K. S.; Snurr, R. Q. Applicability of the BET Method for Determining Surface Areas of Microporous Metal-Organic Frameworks. *J. Am. Chem. Soc.* **2007**, *129*, 8552−8556.
(31) Everett, D. H.; Powl, J. C. Adsorption in Slit-Like and Cylindrical Micropores in the Henry's Law Eegion. A Model for the Microporosity of Carbons. *J. Chem. Soc., Faraday Trans. 1* **1976**, *72*, 619−636.
(32) Do, D. D.; Do, H. D.; Wongkoblap, A.; Nicholson, D. Henry constant and isosteric heat at zero-loading for gas adsorption in carbon nanotubes. *Phys. Chem. Chem. Phys.* **2008**, *10*, 7293−7303.
(33) Steele, W. A.; Halsey, G. D., Jr. The Interaction of Gas Molecules with Capillary and Crystal Lattice Surfaces. *J. Phys. Chem.* **1955**, *59*, 57−65.
(34) Lin, L.-C.; Berger, A. H.; Martin, R. L.; Kim, J.; Swisher, J. A.; Jariwala, K.; Rycroft, C. H.; Bhown, A. S.; Deem, M. W.; Haranczyk, M.; Smit, B. In Silico Screening of Carbon-Capture Materials. *Nat. Mater.* **2012**, *11*, 633−641.
(35) O'Hayre, R. P.; Cha, S.-W.; Colella, W. G.; Prinz, F. B. *Fuel Cell Fundamentals*, 2nd ed.; John Wiley & Sons Ltd: New York, 2009.
(36) Zhou, W.; Wu, H.; Hartman, M. R.; Yildirim, T. Hydrogen and Methane Adsorption in Metal-Organic Frameworks: A High-Pressure Volumetric Study. *J. Phys. Chem. C* **2007**, *111*, 16131−16137.
(37) Fairen-Jimenez, D.; Seaton, N. A.; Düren, T. UnusualAdsorption Behavior on Metal−Organic Frameworks. *Langmuir* **2010**, *26*, 14694−14699.
(38) Gelb, L. D.; Gubbins, K. E. Pore Size Distributions in Porous Glasses: A Computer Simulation Study. *Langmuir* **1999**, *15*, 305−308.
(39) Wang, X. Y.; Lee, K. M.; Lu, Y.; Stone, M. T.; Sanchez, I. C.; Freeman, B. D. Cavity Size Distributions in High Free Volume Glassy Polymers by Molecular Simulation. *Polymer* **2004**, *45*, 3907−3912.
(40) Wilmer, C. E.; Leaf, M.; Lee, C. Y.; Farha, O. K.; Hauser, B. G.; Hupp, J. T.; Snurr, R. Q. Large-Scale Screening of Hypothetical Metal-Organic Frameworks. *Nat. Chem.* **2012**, *4*, 83−89.
(41) Wang, Q.; Johnson, J. K. Molecular Simulation of Hydrogen Adsorption in Single-Walled Carbon Nanotubes and Idealized Carbon Slit Pores. *J. Chem. Phys.* **1999**, *110*, 577−586.
(42) Dailly, A.; Poirier, E. Evaluation of an Industrial Pilot Scale Densified MOF-177 Adsorbent as an On-Board Hydrogen Storage Medium. *Energy Environ. Sci.* **2011**, *4*, 3527−3534.
(43) Richard, M. A.; Bénard, P.; Chahine, R. Gas Adsorption Process in Activated Carbon over a Wide Temperature Range Above the Critical Point. Part 1: Modified Dubinin-Astakhov Model. *Adsorption* **2009**, *15*, 43−51.

(44) Poirier, E.; Dailly, A. Thermodynamics of Hydrogen Adsorption in MOF-177 at Low Temperatures: Measurements and Modelling. *Nanotechnology* **2009**, *20*, 1−6.
(45) Larminie, J.; Dicks, A. *Fuel Cell Systems Explained*, 2nd ed.; John Wiley & Sons Ltd: West Sussex, UK, 2003; pp 289−308.